REGULAR ARTICLE

# Spin-selective electron transmission through self-assembled monolayers of double-stranded peptide nucleic acid

Paul Valerian Möllers[1] | Selma Ulku[2] | Dilhara Jayarathna[2] | Francesco Tassinari[3] | Daniel Nürenberg[1] | Ron Naaman[3] | Catalina Achim[2] | Helmut Zacharias[1]

[1]Center for Soft Nanoscience (SoN), Westfälische Wilhelms-Universität Münster, Münster, Germany

[2]Department of Chemistry, Carnegie Mellon University, Pittsburgh, PA, USA

[3]Department of Chemical and Biological Physics, Weizmann Institute of Science, Rehovot, Israel

**Correspondence**

Paul Valerian Möllers and Helmut Zacharias, Center for Soft Nanoscience (SoN), Westfälische Wilhelms-Universität Münster, Busso-Peus-Str. 10, 48149. Münster, Germany.
Email: paul.moellers@uni-muenster.de; h.zacharias@uni-muenster.de

**Funding information**

National Science Foundation, Grant/Award Number: CHE-1413202; VW Stiftung, Grant/Award Numbers: 88364, 93451, 93454

**Abstract**

Monolayers of chiral molecules can preferentially transmit electrons with a specific spin orientation, introducing chiral molecules as efficient spin filters. This phenomenon is established as chirality-induced spin selectivity (CISS) and was demonstrated directly for the first time in self-assembled monolayers (SAMs) of double-stranded DNA (dsDNA)[1]. Here, we discuss SAMs of double-stranded peptide nucleic acid (dsPNA) as a system which allows for systematic investigations of the influence of various molecular properties on CISS. In photoemission studies, SAMs of chiral, γ-modified PNA show significant spin filtering of up to $P = (24.4 \pm 4.3)\%$ spin polarization. The polarization values found in PNA lacking chiral monomers are considerably lower at about $P = 12\%$. The results confirm that the preferred spin orientation is directly linked to the molecular handedness and indicate that the spin filtering capacity of the dsPNA helices might be enhanced by introduction of chiral centers in the constituting peptide monomers.

**KEYWORDS**

chirality-induced spin selectivity, CISS, monolayer, Mott scattering, peptide nucleic acid, PNA, photoemission, spin filter

## 1 | INTRODUCTION

The discovery of the CISS effect, that is, the spin-selective transmission of electrons through chiral molecules,[1–3] has inspired a variety of application scenarios especially in the fields of spintronics[4,5] and stereochemistry. Recent demonstrations of controlling the selectivity of electrocatalytic reactions,[6–9] and, even more so, the enantioselective adsorption of chiral molecules on magnetic substrates,[10]

[Correction added on 28 January 2021, after first online publication: Paul Valerian Möllers was designated as corresponding author]

represent new paradigms in enantioselective catalysis. Crucially, the CISS effect introduces an absolute reference frame for the orientation of the electron spin at the molecular level.[3] Since its discovery, CISS has been evidenced by different methods, including cyclic voltammetry,[11] magnetic AFM,[12–14] magnetoresistance,[15,16] spin-resolved photoemission,[1] and Hall measurements.[11,17] Besides in dsDNA, CISS was found in oligopeptides,[13,18–20] bacteriorhodopsin,[21–23] alkene-based artificial molecular motors,[16] and further molecular systems.

For helicenes it was shown that the orientation of the preferentially transmitted longitudinal electron spin is

directly related to the helicity of the molecules.[24] Notably, all investigated molecules are as monomer entities spin saturated; that is, they have weak molecular spin-orbit coupling, and consist of only light elements. The theoretical rationalization of the CISS phenomenon has therefore attracted considerable interest in recent years, but a quantitative understanding is still lacking.[25] DNA and most molecules that CISS has been found in have a relatively complex structure. In theoretical models put forth to date, DNA, the most prominent example of molecules that exhibits a very large spin selectivity of up to $P \approx -60\%$ at a length of 78 base pairs,[1] has been represented by model arrangements of atoms aligned along a helical path.[26] Systematic experimental investigations of the influence of various molecular parameters, such as geometry, polarizability, and chemical composition, are thus required to support an understanding of the effect.

A molecule mimicking DNA at reduced complexity that allows to further vary some molecular parameters can be found in peptide nucleic acid (PNA).[27] The chemical structure of PNA is shown in Figure 1 along with DNA. Different from the charged sugar-phosphate groups present in DNA (Figure 1C), the PNA backbone is based on neutral and achiral aminoethylglycine (aeg) monomers (Figure 1A, B), to which the same four canonical nucleobases as in DNA can be attached. PNA hybridizes to both complementary PNA and DNA strands, forming Watson-Crick base pairs.[27–29] The neutral nature of the backbone, and hence the lack of electrostatic repulsion, enhances the thermal stability of the dsPNA and PNA-DNA duplexes over that of dsDNA. The deoxyribose group in the DNA monomer features several chiral centers which dictate the double helix structure of the dsDNA duplexes. The aeg-based monomers are achiral; hence, dsPNA duplexes can adopt both right- and left-handedness. A preference for a specific handedness can be induced in dsPNA either by the introduction of a chiral group, for example, a chiral lysine residue, at the C-terminus of PNA,[30] or a substituent group in the γ position of the aeg backbone. These modifications render the primary structure chiral,[31] as indicated in Figure 1B. If both approaches are applied simultaneously, two influences are present that can direct the handedness in conflicting directions.[32] We have synthesized PNAs that contain chiral

monomers with high affinity for metal ions whose chiral induction effect prevails at standard conditions, but is turned off by addition of $Cu^{2+}$ ions, causing a reversal of the helical sense.[32,33] Such structures whose handedness can be switched could be used in the creation of systems with switchable spin selectivity.

The previously reported values of the helical parameters of dsPNA, γ-modified dsPNA, and dsDNA are summarized in Table 1. The table also includes the parameters for PNA-DNA and γPNA-DNA heteroduplexes. The values for dsPNA and dsγPNA were obtained in NMR studies and subsequent molecular dynamics simulations.[29,34,36] Compared to the 'B' conformation of dsDNA which has a pitch of 3.4 nm per helical turn, dsPNA adopts a P-type helix which is considerably less twisted at 7.8 nm per helical turn. The helical conformation of dsγPNA exhibits structural features of both dsPNA and dsDNA[38]; the pitch is slightly reduced to 6.4 nm per helical turn. One helical turn corresponds to 21 and 22 base pairs in dsPNA and dsγPNA, respectively, whereas in dsDNA, it includes only 10 base pairs. The pitch of the PNA-DNA heteroduplex structures lies between the values of the respective homoduplex structures.

In this contribution, we demonstrate the spin selectivity in electron transmission through SAMs of dsPNA by directly measuring the resulting photoelectron spin polarization. In a first step, we studied dsPNA consisting of only achiral monomers, as well as γPNA-PNA duplexes that feature several chiral monomers. For each structure both left- and right-handed forms were investigated. Since the method has been employed earlier, a direct comparison can be drawn between dsPNA duplexes and, for example, dsDNA,[1] oligopeptides,[18] bacteriorhodopsin,[21] and hepta-helicene.[24]

## 2 | MATERIALS AND METHODS

### 2.1 | PNA duplex structure and characterization

The investigated 20 base pair PNA duplexes were generated by hybridization of two single-stranded PNA
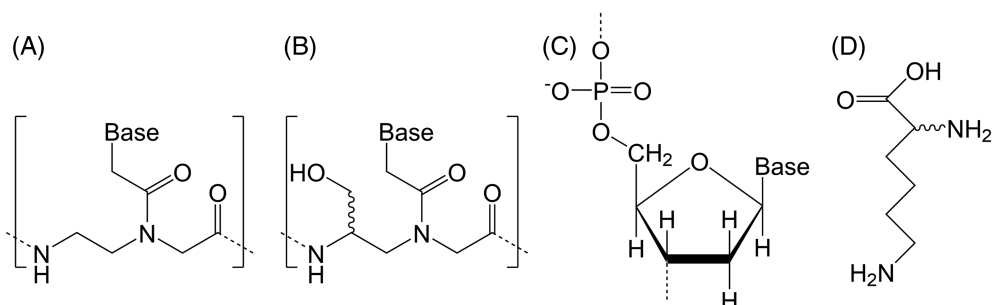


**FIGURE 1** Structure of (A) the aminoethylglycine (aeg), (B) the γ-modified aeg, and (C) the deoxyribose-phosphate monomers in the backbones of PNA, γPNA, and DNA, respectively; (D) the structure of lysine

**TABLE 1** Helical parameters of self-complimentary PNA and DNA double helices

| | Pitch (nm/helical turn) | Bp/helical turn | Base pair rise (nm/bp) | Diameter (nm) |
|---|---|---|---|---|
| dsPNA | 7.8 | 21[34] | 0.37[34] | 2.8[34,35] |
| dsγPNA | 6.4 | 22[36] | 0.29[36] | |
| dsDNA (B conformation) | 3.4[37] | 10[35] | 0.34 | 2.4[34] |
| PNA-DNA | 4.2[38] | 13[38] | 0.32 | 2.3[38] |
| γPNA-DNA[a] | 4.8/4.5 | 15.1/15.5[29] | 0.32/0.29[29] | |

[a]In the NMR study,[29] two distinct coexisting duplex conformations were found.

(ssPNA) decamers to a 20-mer template PNA strand. All duplexes feature the same sequence of base pairs which is shown in Section S1 of the supporting information (SI). The molecular weights of the different constituent strands were characterized by MALDI ToF mass spectrometry and were found to be in good agreement with the calculated values (see Section S1 in the SI). The dsPNAs were prepared by keeping solutions containing the appropriate equivalents of ssPNA in a 1:1 mixture of acetonitrile and pH = 7.2, 20 mM phosphate buffer at 90°C for 10 min, followed by cooling to 15°C at a rate of 1°C min⁻¹. In the duplexes, the strands are aligned antiparallel; that is, the base sequences are such that the C end of one strand is aligned with the N end of the complementary strand. Antiparallel dsPNA duplexes were shown to be substantially more thermally stable than parallel duplexes.[30] In all duplexes, the C end of one of the decamer PNAs is thiolized to covalently bind the duplexes onto the gold substrate during surface functionalization. In the unmodified dsPNA duplexes, L- or D-lysine groups located at the C end of the template strand and at the N end of the nonthiolized decamer induce a preference for left- or right-handed double helices, respectively. In the γPNA-PNA duplexes, the nonthiolized decamers feature a lysine group at the C end, instead, and serine-derived hydroxymethyl side groups[31] at the γ position in three of the 10 monomers. These groups, whose structure is shown in Figure 1B, render the respective monomers chiral and sterically induce a preference for left- (right-) handed duplexes in case of D (L)-serine-derived substituents. The effect of the γ-modified monomers is dominant over the effect of terminal D- or L-lysine groups also present in the duplex. In the present study, right-handed (P) γPNA-PNA duplexes contained L-lysine and L-serine-derived γ-substituents; in left-handed (M) γPNA-PNA duplexes the enantiomers of both groups were opposite.

The formation and chirality of all four duplexes was confirmed by CD measurements which were acquired in solutions prepared in pH 7.0, 10 mM sodium phosphate buffer. The spectra are shown in Figure 2. Both dsPNA with D-lysine groups and γPNA-PNA with L-lysine groups and γL-serine-modified monomers exhibit distinct exciton

coupling pattern with local minima at about 240 and 280 nm indicative of helical stacking of the bases.[29] Since the achiral backbone of PNA has no well-defined helical conformation, the significant CD confirms the duplex formation.[29] The positive peak below 220 nm, which is assigned to the $n - \pi^*$ transition of the amides in the backbone[31,39] and the positive feature at about 255 nm are indicative of right-handed (P) helical conformations.[40] Nominally left-handed (M) dsPNA and γPNA-PNA duplexes exhibit spectra which are in good approximation the mirror images of these spectra, confirming their reversed helicity. In γPNA-PNA the absolute CD magnitude shows with 18 mdeg at 255 nm (right scale) a value four times larger than observed for unmodified dsPNA duplexes, regardless of the helical sense. This most likely reflects the differences in the strength of the chiral induction effect exerted by the terminal lysine and the γ-modified monomers. Small asymmetries in the CD
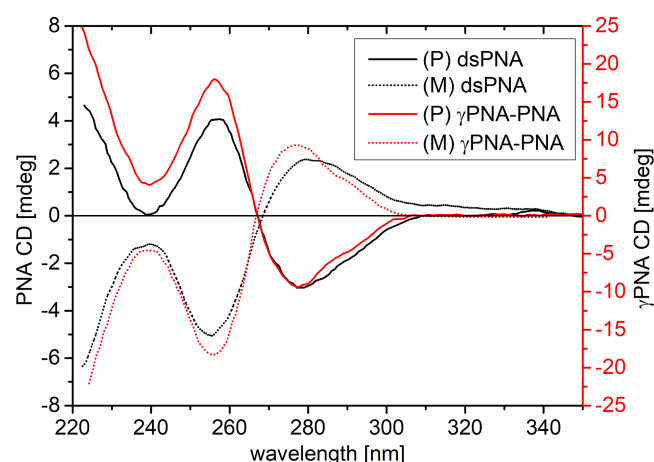


**FIGURE 2** CD spectra of left- and right-handed dsPNA with L (D)-lysine as chiral seeds and γPNA-PNA duplexes with D (L)-lysine and D (L)-γ-modified monomers, respectively. The spectra were acquired for 3 μM solutions of the duplexes in pH 7.0 10 mM sodium phosphate buffer. Note that the CD spectra were acquired for duplexes that were identical to those used in the photoemission studies except that they lacked the thiol linkers to avoid oxidation of the thiol during the measurements. The approximate error is ±1 mdeg

spectra are due to minor differences in the purity of the L and D amino acids used in the synthesis.

## 2.2 | Monolayer preparation and characterization

Polycrystalline gold surfaces were functionalized with self-assembled monolayers of the various PNA duplexes. The duplexes were covalently attached to the surfaces through the thiolized C-end of the decamer. The gold surfaces were prepared via e-beam evaporation on either a silicon or a fused silica wafer with a thin (5–8 nm) titanium adhesion layer. The thickness of the gold layer was 120 nm on the silicon wafers and 20 nm on the fused silica substrates. The gold-covered fused silica slides were introduced as a substrate in a fraction of the samples to allow for irradiation with a laser from the back side of the sample, in an attempt to reduce possible UV radiation damage in the SAMs. The gold surfaces were cleaned before the SAM incubation by boiling them for 10 min in acetone and then for the same time in ethanol, followed by a 5-min oxygen plasma treatment and a 40-min incubation in ethanol. Then, the surfaces were dried under a nitrogen flow and immediately put in contact with the PNA solution.

For the formation of the monolayers, the gold surfaces were incubated with 40 μl of the 20 μM dsPNA solution for 40 h at 27°C under a water saturated atmosphere to avoid evaporation of the solvent from the surface. Afterward, the surfaces were washed twice with pH = 7.2, 20 mM phosphate buffer, twice with water and then dried under a nitrogen flow. The self-assembled PNA monolayers were characterized by ellipsometry and PM-IRRAS spectroscopy measurements. The ellipsometric data are reported in Table 2.

The typical polarization modulation infrared reflection-absorption spectra (PM-IRRAS) of the different monolayers are reported in Figure 3. No significant deviations between the different samples are apparent, which indicates a consistent SAM quality. No change in intensity or frequency is observed between 3000 and 2800 cm$^{-1}$, corresponding to the CH and CH$_2$ stretching modes, for the SAMs of different duplexes. The region from 1750 to 1550 cm$^{-1}$ shows the in-plane double-bond vibrations of the nucleic bases. Although small
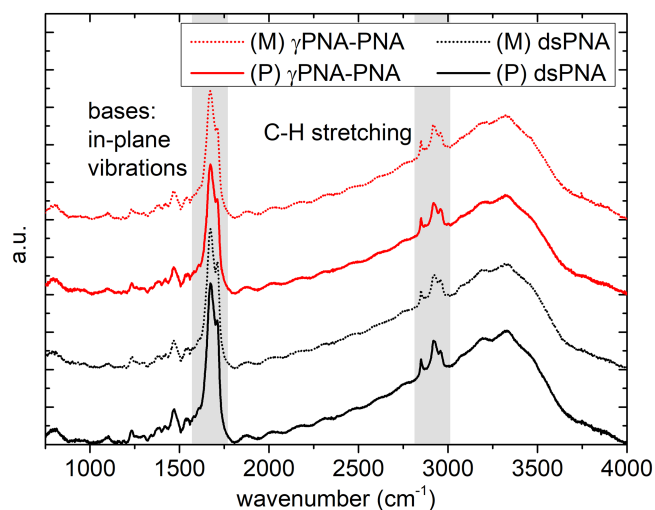


**FIGURE 3** PM-IRRAS spectra of monolayers of dsPNA and γPNA-PNA duplexes with both (M) and (P) handedness

differences in intensity are seen in this region between the different monolayers, no clear dependence of the changes on the duplex structure can be derived. The peptide backbone signature peaks of amide I (C=O stretch, 1650 cm$^{-1}$) and amide II (NH deformation, 1540 cm$^{-1}$) also appear in this region; this complicates the data analysis and prevents us from gaining an exact understanding on the molecular orientation. However, the presence of the intense in-plane double-bond vibrations of the nucleic bases shows that the bases are considerably tilted with respect to the normal of the surface, which is compatible with the idea of the presence of two different phases in the monolayer, rather than of a uniformly tilted orientation for all duplexes in the SAM.

The theoretical length of the PNA duplexes can be roughly estimated using the helical parameters of the different PNA structures presented in Table 1. The dsPNA and the dsγPNA have theoretical lengths of 7.4 and 5.8 nm, respectively. The measured thickness of the SAMs of γPNA-PNA is indeed lower than that of dsPNA, but for both SAMs it is lower than the theoretical length of the duplexes. Assuming a full coverage of the surface during monolayer formation, there are two possible explanation for this discrepancy. First, the helical axis of the duplexes may be tilted rather than parallel with respect to the normal to the surface. Second, it may be that some of the

**TABLE 2** Average thickness value of the SAMs of various PNA duplexes measured by ellipsometry

|  | (M) dsPNA | (P) dsPNA | (M) γPNA-PNA | (P) γPNA-PNA |
|---|---|---|---|---|
| Average thickness (nm) | 4.8 (0.3) | 5.2 (0.5) | 4.3 (0.1) | 4.4 (0.1) |
| Approx. lying-down fraction (%) | 57 | 48 | ≲50 | ≲50 |

*Note*: Each value is the average of six different samples; the standard deviation is reported in the parentheses. In second row, the approximate fraction of lying-down duplexes, calculated from the thickness values, is given.

duplexes have their helical axis perpendicular to the surface while the rest "lie down" on the surface, forming two phases with different relative thicknesses in the monolayer. There is precedence for the latter situation in SAMs of PNA[41] but these two possibilities are hard to distinguish experimentally. If we assume that the second explanation applies and that theoretical thickness for the lying down phase is given by the diameter of the dsPNA helix, which is 2.8 nm, the presence in the SAMs of a "lying-down" phase of ~57% and ~48%, in the SAMs of (M) PNA and (P) PNA, respectively, would explain the measured thicknesses. At 0.3 and 0.5 nm, the standard deviations of these measurements are rather high, though, and there is large variability from sample to sample. For the γPNA-PNA duplexes, the ellipsometry results are more consistent between (M) and (P) SAMs and between individual samples, suggesting that the γ-substituted structures form more well-defined monolayers. For these layers, assuming a diameter of the helix of 2.8 nm, we obtain a "lying-down" phase of ≲50% for both enantiomers. Since the duplexes are likely to homogeneously adopt a nonzero tilt angle with respect to the surface normal, these calculated fractions represent worst case limits. It has been shown that the fraction of lying-down molecules depends on the surface coverage.[42] The results thus suggest a similar surface coverage on all samples. X-ray photoelectron spectra of the investigated samples, shown in Figure S2 in the SI, support this conclusion. On average, the intensity of the nitrogen 1s peak relative to the gold 4f peaks is about 10.8% for the dsPNA samples and 7.6% for γPNA-PNA. Although nitrogen is abundant in the PNA molecules, no nitrogen signal is present in the spectrum of the unfunctionalized (but neither sputtered nor annealed) gold substrate, where the carbon 1s signal certainly arises from contamination. The N 1s intensities are, however, well correlated with the chemically shifted C 1s peak at about 288 eV which arises from the N-C=O bonds in the aeg backbone. This allows ruling out that the numbers reflect mainly random fluctuations, and the nitrogen signal can be employed as a measure of the relative surface coverage. As the nominal nitrogen content of dsPNA and γPNA-PNA is identical, these results provide further evidence that the (macroscopically averaged) surface coverage is similar for all samples. If the intrinsic SAM densities of dsPNA and γPNA-PNA duplexes were different, the density would most likely be higher for nonmodified dsPNA based on these numbers. This is in line with the investigations of the respective duplex geometries, which show that γPNA-PNA is bulkier than unmodified dsPNA.[36]

The electronic structure of the SAM adsorbed on the 20-nm-thick gold substrate was further elucidated in He I UPS measurements which can be found in Section S2 of the SI. The energy level diagram derived from the data is shown in Figure 4. From the spectra, the substrate work function was determined to $\Phi = 4.62$ eV. This value is lower than literature values for bulk gold due to the low thickness of the gold film. Functionalization of the surface with the dsPNA SAM introduces a surface dipole $\Delta\Phi$ which reduces the work function and manifests in a shift of the secondary edge of the photoelectron spectrum. From the position of the highest occupied MO of the SAM, the ionization energy of the dsPNA duplexes is determined to be 7.40 eV. This result closely resembles values reported for single-stranded PNA.[43]

## 2.3 | Spin-resolved photoemission studies

The spin filtering capability of the PNA duplexes was assessed by measuring the average spin orientation of photoelectrons transmitted through PNA SAMs using a previously described experimental setup.[1,24] The photoelectrons were excited from the gold substrate by laser pulses at 213 nm ($h\nu = 5.83$ eV) with a repetition rate of 20 kHz, generated as the fifth harmonic of a Nd:YVO$_4$ laser. A fraction of about $10^{-4}$ of the incident light is absorbed within the monolayer. Since the photon energy is well below the molecular ionization potential, the photoelectrons originate solely from the gold substrate. The pulse energy was in the range of 10–100 pJ over a pulse duration of about 200 ps and an e$^{-2}$ area of approximately 0.3 mm$^2$, corresponding to a peak intensity of about 100 Wcm$^{-2}$ at which two-photon processes can be neglected. The laser impinged normal onto the sample surface. Photoelectrons with a maximum kinetic energy of about 1 eV were extracted normal to the surface and
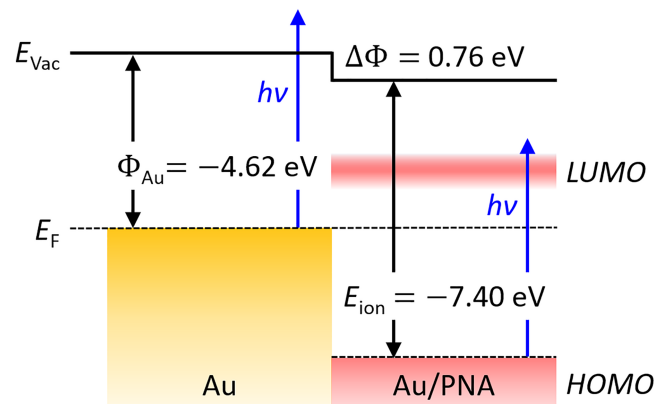


**FIGURE 4** Energy level diagram of the functionalized gold surface, determined from He I UPS measurements. At 7.40 eV, the ionization energy of the adsorbed PNA is higher than the photon energy $h\nu = 5.83$ eV. Hence, no photoemission occurs from the adsorbed SAM. The energetic position of the lowest unoccupied MO was not determined

guided into a Mott polarimeter to measure the average longitudinal spin orientation of the electrons. Inside the polarimeter, the photo-electrons were accelerated toward a scattering target at +50 kV. Two detectors are placed at ±120° with respect to the incident electron beam. The asymmetry in the scattering intensities at both detectors is a measure of the average spin orientation of the incident electrons (additional information is provided in Section S3 of the SI). Since the polarimeter is only sensitive to the transversal component of the spin polarization, the electron beam was bent by 90° prior to the measurement. In the resulting configuration the initially longitudinal spin component along the surface normal of the samples is measured. A positive polarization value corresponds to a spin aligned parallel to the electron velocity vector.

A polycrystalline gold substrate was mounted as a reference directly beneath the sample to determine instrumental asymmetries and calibrate for zero spin polarization. The polarization of the incident laser light was altered between linear, clockwise (cw), and counter-clockwise (ccw) circular by rotation of a quarter-wave plate (QWP). The direction of circular polarization is defined relative to the spin quantization axis, that is, along the surface normal of the sample. At each QWP position, about $10^6$ laser pulses were applied and $10^5$ electrons were detected. The sample position was interchanged in vacuum between the functionalized surface and the bare gold substrate after each full QWP rotation.

Before and after the measurement procedure on each sample, the spin polarization of photoelectrons emitted from a sputter-cleaned Au(111) single crystal was determined to confirm the correct alignment of the polarimeter. The results were regarded valid and kept only if spin polarization values of about ±25% for cw and cw circularly polarized light,[44] respectively, were measured before and after the PNA measurement.

# 3 | RESULTS AND DISCUSSION

## 3.1 | Measurement results

From the scattering intensities $I_\pm$ of the two detectors the spin polarization $P$ is calculated as $P = (I_+ - I_-)/(I_+ + I_-) \cdot S^{-1}$, where $S = 0.18$ is the Sherman function which quantifies the analyzing power of the polarimeter. The measurement results are shown in Figure 5 as histograms of the spin polarization values obtained in each run of about $10^6$ laser pulses. For each measurement procedure, three histograms are given, corresponding to the different polarization states of the incident laser light. The spin polarization values are extracted as the expectation values of Gaussian curves fitted to the distributions; the stated error corresponds to the standard deviation. Figure 5C shows the results of a measurement on a nonfunctionalized polycrystalline gold substrate. The intrinsic spin-orbit coupling in polycrystalline gold manifests in small nonzero spin polarizations which are measured if the photoelectrons are excited with circularly polarized light. These values depend on the local crystallite structure of the gold and therefore vary
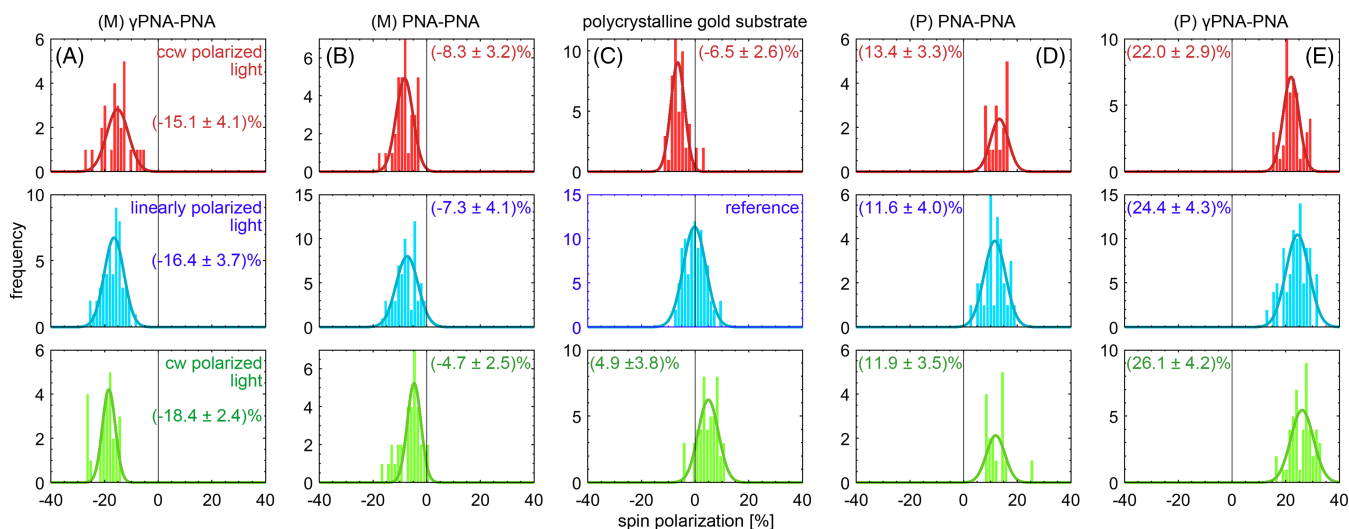


**FIGURE 5** Spin polarization distributions of photoelectrons transmitted through a monolayer of (A) left-handed, double-stranded 20 base pair γPNA-PNA duplexes, (B) left-handed unmodified dsPNA, (D) right-handed dsPNA and (E) right-handed γPNA-PNA duplexes. Column (C) shows a measurement on a blank substrate, with the highlighted distribution used to define the point of zero spin polarization. The three rows correspond to excitation with ccw (red), cw (green) circularly, and linearly (blue) polarized light. The curves are Gaussian functions fitted to the data

slightly between the individual samples. Upon excitation with linearly polarized light, always unpolarized photoelectrons are emitted from the substrate. These electrons are used as the reference to correct for instrumental asymmetries.

The results presented in Figure 5A and B show negatively spin-polarized photoemission from the surfaces functionalized with (M) dsPNA and (M) γPNA-PNA. Correspondingly, positive spin polarizations are measured for (P) dsPNA and (P) γPNA-PNA (Figure 5D,E). As a possible source for the observed electron spin polarization a modification of the electronic structure of the substrate at the gold–SAM interface has been proposed.[45] The data discussed in the present work do not allow to disprove this view. Previous studies, however, reported spin-polarized photoemission even in case of physisorbed molecules, and furthermore found the polarization values to be largely independent of the substrate material.[24] Although modifications of the electronic structure may contribute to the phenomenon, we attribute the spin polarization primarily to spin-selective electron transmission, that is, a spin-filtering process in the helical molecules, which is in line with the currently established interpretation.[25]

For all functionalized surfaces in Figure 5, the electron spin polarization is independent from the light polarization within the error margins. Hereafter, we discuss the spin polarization obtained for excitation with linearly polarized light, thus for initially unpolarized electrons emitted from the polycrystalline gold substrate.

In Figure 5B, the spin polarization values obtained from a sample covered with a monolayer of 20 base pair long, unmodified (M) dsPNA helices are shown. Compared to the nonfunctionalized substrate, the respective distributions are shifted toward negative values. After transmission through the monolayer, the initially unpolarized photoelectrons exhibit an average spin polarization of $P = (-7.3 \pm 4.1)$%, indicating that electrons with spins oriented antiparallel to the electron velocity vector are preferentially transmitted through the layer. Distributions measured on a monolayer of right-handed (P) dsPNA are given in Figure 5D. At $P = (11.6 \pm 4.0)$%, the polarization values are shifted toward positive values relative to the bare substrate. A substantially larger spin polarization value of $P = (-16.4 \pm 3.7)$% was observed on a monolayer of (M) γPNA-PNA helices, see Figure 5A. A SAM of right-handed γPNA-PNA exhibited reversed and higher spin selectivity at $P = (24.4 \pm 4.3)$%, as shown in Figure 5E. According to this value, up to 62% of the electron spins are aligned parallel to the electron velocity vector even if the photoelectrons from the substrate are initially unpolarized. For each sample, a second measurement on a different position on the monolayer was

conducted, which is shown in Section S4 of the SI. In general, this second, independent set of measurements results in similar spin polarization values as the first one. A second measurement on the (M) γPNA-PNA monolayer yielded $P = (-7.6 \pm 3.3)$%; on the right-handed (P) monolayer $P = (18.6 \pm 3.5)$% was measured. In additional measurements on the (M) and (P) dsPNA monolayers spin polarization values of $P = (-6.7 \pm 4.4)$% and $P = (6.6 \pm 3.0)$%, respectively, were obtained.

## 4 | DISCUSSION

These results for PNA support the notion that spin-selective electron transmission is indeed a very general and robust phenomenon present in a wide range of helical molecules and for both bound and unbound electrons. As AFM conduction measurements have shown that CISS is not a collective phenomenon but a property of the individual molecules in the monolayers,[14] we consider here only the maximum spin polarization values measured for each duplex, shown in Figure 5.

Several conclusions can be drawn from the results presented above. A clear correlation between the helical sense of the duplexes and the preferentially transmitted electron spin direction is observed. For right-handed (P) dsPNA and (P) γPNA-PNA helices, positive spin polarization values were measured; that is, electrons with the spin direction aligned parallel to the momentum are preferentially transmitted through the layers. Monolayers consisting of left-handed (M) helices, both dsPNA and γPNA-PNA, were found to more likely transmit electrons with antiparallel oriented spins. Interestingly, this is opposite to right-handed dsDNA,[1] right-handed oligopeptide α-helices,[18] and right-handed overcrowded alkenes,[16] which preferentially transmit antiparallel oriented spins. However, the relation between handedness and spin direction is the same as was found in heptahelicene[24] and bacteriorhodopsin α-helices,[21] where spins parallel to the momentum are preferred in the right-handed (P) configurations, as well.

The measurements shown in Figure 5 suggest that γPNA-PNA duplexes act as very efficient spin filters. In contrast to unmodified PNA, γPNA included several monomers with a stereogenic center in the backbone and displayed a significantly stronger CD intensity. In the present study, the maximum spin selectivity found in γPNA-PNA was two to three times higher than what was found in dsPNA. This correlates well with the relative magnitudes of the spectral features in the CD of the two duplexes (Figure 2). However, as the employed photon energy is not sufficient to directly excite the molecules, the solution CD spectra and that of adsorbed PNA cannot

be compared directly. Because absorption in the SAM does not lead to photoemission, the CD might be an indication that spin selectivity is occurring, but no direct relationship via the light absorption is given.

As the base sequences for both dsPNA and γPNA-PNA are identical (see SI), a possible electron transfer through the bases is not expected to lead to differences in the spin polarization. Although it is known that dsγPNA duplexes are less flexible than unmodified dsPNA duplexes,[36,46] the different magnitudes of the spin selectivity may be related to the different helical parameters of dsPNA and dsγPNA. The pitch of dsγPNA, with $l = 6.4$ nm, is considerably shorter than that of unmodified dsPNA ($l = 7.8$ nm, see Table 1). Since the diameter of the helical backbone can be assumed to be similar at about 2.8 nm,[35] this reduced pitch could be a cause of the enhanced spin polarization in γPNA-PNA duplexes. An experiment of Kiran et al. in which the pitch of helical oligopeptides was artificially reduced by exerting a force onto the molecules, led, by contrast, to a smaller spin polarization value.[13] As the initial ratio of pitch to radius of the molecules are smaller than 1 for the oligopeptides and larger than 1 for γPNA-PNA the results are consistent with one another if one assumes a ratio of 1:1 as ideal for CISS.[13] Moreover, it could also be that the chiral centers in some of the monomers play a crucial role. In the present study in the γPNA-PNA duplexes one decamer has three γ-substituted monomers. It is expected that the addition of γ-substituent groups to even more monomers would, from a certain relative amount on, not significantly influence the helical parameters of the γPNA-PNA duplexes any further. Hence, measurements on samples with more chiral monomers in the PNA backbones could elucidate whether the observed enhancement of CISS in γPNA-PNA compared to dsPNA is due to the mere presence of chiral monomers or due to the different helical conformation of γPNA-PNA compared to dsPNA.

On the other hand, the pitch of dsγPNA is much larger than that of dsDNA ($l = 3.4$ nm, see Table 1). A dsPNA unit consisting of 20 base pairs thus corresponds to a bit less than one helical turn. At this length γPNA-PNA exhibits a spin selectivity of about $P = 24\%$. A 26 base pair dsDNA duplex has 2.6 helical turns and a length of 8.8 nm and showed a selectivity of about $|P| = 12\%$.[1] For dsDNA lengths ranging from 26 to 78 bp, the spin polarization per length is about 2–3%nm$^{-1}$, which is approximately half the value determined for γPNA-PNA in the present study. However, these numbers might also reflect the inherent monolayer density, which, at least for single strands, is higher for ssPNA layers than it is for ssDNA layers.[47] Unmodified dsPNA is roughly half as efficient as dsDNA when the spin

polarization is normalized to the duplex length. Spin polarizations of $|P| = 17\%$ were previously determined for oligopeptide helices with a length of 2.8 nm[18] which, in this respect, are even more efficient than γPNA-PNA, surpassed by heptahelicene layers which so far exhibited the largest spin selectivity per length[24] at up to $|P| = 9\%$ at a thickness of 0.22 nm.[48]

When comparing absolute spin polarizations of samples with different entities some precaution must be observed. Even in case of the most promising γPNA-PNA monolayer and despite the macroscopically large measurement area of about 0.3 mm$^2$, the measured spin polarization values varied by as much as 30% over the surface area. This suggests that creating dsPNA-functionalized surfaces of consistent quality, or maintaining their quality throughout the measurement procedure, remains challenging. In magnetoresistance studies of dsDNA SAMs, it was found that a reduction of the electrode size from 50 to 10 μm lead to an approximately tenfold increase of the magnetoresistance.[49] Therefore, imperfections of the monolayers are likely to reduce the measured spin selectivity. It is reasonable to assume that reduced spin polarization values reflect the characteristics and imperfections of the specific samples rather than the properties of the duplexes themselves.

As demonstrated by the results presented in this paper, PNA allows for the systematic investigation of the dependence of the spin polarization on the pitch of the molecule while maintaining the atomic constituents largely unchanged. Entities with different geometries can be generated by fusing PNA and γPNA strands onto a DNA strand (see Table 1). Since PNA is more flexible than DNA, it adopts a structure similar to that of B-DNA in PNA-DNA heteroduplexes,[40] specifically regarding the geometry of the backbone.[38] Heteroduplexes of γPNA and DNA, on the other hand, resemble more closely the helical structure of A-type DNA, with a significant displacement of the bases away from the helical axis of the duplex.[29] Measurements of the molecular conductance of dsPNA duplexes with different structures and different linker molecules[46] have already shown that the molecular conductance must be treated as a (semi-) coherent sum of charge injection, transport, and escape. Therefore, the influence of both structure and position of the linker group, which can be attached to the template strand instead of the decamer, is of interest, as well. The surface dipole determined in the present study corresponds to an electric field strength as high as 10$^8$ V m$^{-1}$ within the SAM. Although theoretical studies[50,51] have identified a large electric dipole field as a crucial condition for the occurrence of CISS, its influence has not yet been assessed experimentally.

Another interesting route is to study the influence of the base sequence on CISS. Previous studies showed that of the four canonical bases, guanine preferentially captures low-energy electrons,[47] which is likely to affect the spin-selective electron transmission. The guanine content in the abovementioned 26 base pair dsDNA[1] was 8%, while the guanine content in the dsPNA duplexes investigated in the present work is 30%. Hence, as a starting point for future work, dsDNA and dsPNA with identical sequences of base pairs and varying guanine content will be investigated.

In conclusion, we have demonstrated spin-selective photoelectron transmission in dsPNA SAMs and confirmed that the preferentially transmitted spin orientation is directly linked to the molecular helicity. The results suggest that the spin polarization is enhanced by introduction of chiral centers into the constituting monomers. However, the influence of the respective local monolayer quality requires further investigation. Compared to dsDNA, the spin polarization per length is doubled in γPNA-PNA duplexes. The possibility to create heteroduplexes allows to investigate structures with different helical conformations while largely preserving the chemical composition, making PNA an interesting system for further systematic studies of the CISS effect.

## DATA AVAILABILITY STATEMENT
The data that support the findings of this study are available from the corresponding author upon reasonable request.

## ORCID
*Paul Valerian Möllers* https://orcid.org/0000-0002-6916-7664

## REFERENCES
1. Göhler B, Hamelbeck V, Markus TZ, et al. Spin selectivity in electron transmission through self-assembled monolayers of double-stranded DNA. *Science*. 2011;331(6019):894-897.
2. Mayer S, Kessler J. Experimental verification of electron optic dichroism. *Phys Rev Lett*. 1995;74(24):4803-4806.
3. Naaman R, Paltiel Y, Waldeck DH. Chiral molecules and the electron spin. *Nature Reviews Chemistry*. 2019;3(4):250-260.
4. Al-Bustami H, Koplovitz G, Primc D, et al. Single nanoparticle magnetic spin memristor. *Small*. 2018;14(30):1801249.
5. Naaman R, Waldeck DH. Spintronics and chirality: spin selectivity in Electron transport through chiral molecules. *Annu Rev Phys Chem*. 2015;66(1):263-281.
6. Mtangi W, Kiran V, Fontanesi C, Naaman R. Role of the electron spin polarization in water splitting. *J Phys Chem Lett*. 2015;6(24):4916-4922.
7. Mtangi W, Tassinari F, Vankayala K, et al. Control of electrons' spin eliminates hydrogen peroxide formation during water splitting. *J Am Chem Soc*. 2017;139(7):2794-2798.
8. Zhang W, Banerjee-Ghosh K, Tassinari F, Naaman R. Enhanced electrochemical water splitting with chiral molecule-coated $Fe_3O_4$ nanoparticles. *ACS Energy Lett*. 2018;3(10):2308-2313.
9. Ghosh KB, Zhang W, Tassinari F, et al. Controlling chemical selectivity in electrocatalysis with chiral CuO-coated electrodes. *J Phys Chem C*. 2019;123(5):3024-3031.
10. Ghosh KB, Ben Dor O, Tassinari F, et al. Separation of enantiomers by their enantiospecific interaction with chiral magnetic substrates. *Science*. 2018;360(6395):1331-1334.
11. Mishra S, Poonia VS, Fontanesi C, Naaman R, Fleming AM, Burrows CJ. Effect of oxidative damage on charge and spin transport in DNA. *J Am Chem Soc*. 2019;141(1):123-126.
12. Ben Dor O, Yochelis S, Radko A, et al. Magnetization switching in ferromagnets by adsorbed chiral molecules without current or external magnetic field. *Nat Commun*. 2017;8(1):14567.
13. Kiran V, Cohen SR, Naaman R. Structure dependent spin selectivity in electron transport through oligopeptides. *J Chem Phys*. 2017;146(9):092302.
14. Xie Z, Markus TZ, Cohen SR, Vager Z, Gutierrez R, Naaman R. Spin specific electron conduction through DNA oligomers. *Nano Lett*. 2011;11(11):4652-4655.
15. Kiran V, Mathew SP, Cohen SR, Hernández Delgado I, Lacour J, Naaman R. Helicenes—A new class of organic spin filter. *Adv Mater*. 2016;28(10):1957-1962.
16. Suda M, Thathong Y, Promarak V, et al. Light-driven molecular switch for reconfigurable spin filters. *Nat Commun*. 2019;10(1):2455.
17. Ben Dor O, Morali N, Yochelis S, Baczewski LT, Paltiel Y. Local light-induced magnetization using nanodots and chiral molecules. *Nano Lett*. 2014;14(11):6042-6049.
18. Kettner M, Göhler B, Zacharias H, et al. Spin filtering in electron transport through chiral oligopeptides. *J Phys Chem C*. 2015;119(26):14542-14547.
19. Aragonès AC, Medina E, Ferrer-Huerta M, et al. Measuring the spin-polarization power of a single chiral molecule. *Small*. 2017;13(2):1602519.
20. Tassinari F, Jayarathna DR, Kantor-Uriel N, Davis VV, Achim C, Naaman R. Chirality dependent charge transfer rate in oligopeptides. *Adv Mater*. 2018;30(21):1706423.
21. Mishra D, Markus TZ, Naaman R, et al. Spin-dependent electron transmission through bacteriorhodopsin embedded in purple membrane. *Proc Natl Acad Sci*. 2013;110(37):14872-14876.

22. Varade V, Markus TZ, Vankayala K, et al. Bacteriorhodopsin based non-magnetic spin filters for biomolecular spintronics. *Phys Chem Phys*. 2018;20(2):1091-1097.

23. Einati H, Mishra D, Friedman N, Sheves M, Naaman R. Light-controlled spin filtering in bacteriorhodopsin. *Nano Lett*. 2015; 15(2):1052-1056.

24. Kettner M, Maslyuk VV, Nürenberg D, et al. Chirality-dependent electron spin filtering by molecular monolayers of helicenes. *J Phys Chem Lett*. 2018;9(8):2025-2030.

25. Naaman R, Paltiel Y, Waldeck DH. Chiral molecules and the spin selectivity effect. *J Phys Chem Lett*. 2020;11(9):3660-3666.

26. Gutierrez R, Díaz E, Gaul C, Brumme T, Domínguez-Adame F, Cuniberti G. Modeling spin transport in helical fields: Derivation of an effective low-dimensional Hamiltonian. *J Phys Chem C*. 2013;117(43):22276-22284.

27. Egholm M, Buchardt O, Nielsen PE, Berg RH. Peptide nucleic acids (PNA). Oligonucleotide analogues with an achiral peptide backbone. *J Am Chem Soc*. 1992;114(5):1895-1897.

28. Nielsen PE, Egholm M. An introduction to peptide nucleic acid. *Curr Issues Mol Biol*. 1999;1:89-104.

29. Yeh JI, Shivachev B, Rapireddy S, et al. Crystal structure of chiral γPNA with complementary DNA strand: Insights into the stability and specificity of recognition and conformational preorganization. *J Am Chem Soc*. 2010;132(31): 10717-10727.

30. Wittung P, Nielsen PE, Buchardt O, Egholm M, Nordén B. DNA-like double helix formed by peptide nucleic acid. *Nature*. 1994;368(6471):561-563.

31. Dragulescu-Andrasi A, Rapireddy S, Frezza BM, Gayathri C, Gil RR, Ly DH. A simple γ-backbone modification preorganizes peptide nucleic acid into a helical structure. *J Am Chem Soc*. 2006;128(31):10258-10267.

32. Sargun A, Fang Y, Achim C. The disobeying 'soldier': Use of an achiral group to modulate chiral induction in PNA duplexes. *Chimia*. 2018;72(6):368-374.

33. Bezer S, Rapireddy S, Skorik YA, Ly DH, Achim C. Coordination-driven inversion of handedness in ligand-modified PNA. *Inorg Chem*. 2011;50(23):11929-11937.

34. He W, Hatcher E, Balaeff A, et al. Solution structure of a peptide nucleic acid duplex from NMR data: Features and limitations. *J Am Chem Soc*. 2008;130(40):13264-13273.

35. Rasmussen H, Kastrup JS, Nielsen JN, Nielsen JM, Nielsen PE. Crystal structure of a peptide nucleic acid (PNA) duplex at 1.7 Å resolution. *Nat Struct Biol*. 1997;4(2):98-101.

36. He W, Crawford MJ, Rapireddy S, et al. The structure of a γ-modified peptide nucleic acid duplex. *Mol Bio Syst*. 2010;6: 1619-1629.

37. Heinrich PC, Müller M, Graeve L. *Löffler/Petrides Biochemie und Pathobiochemie*. 9 Berlin, Heidelberg: Springer; 2014:131.

38. Erikson M, Nielsen PE. Solution structure of a peptide nucleic acid-DNA duplex. *Nat Struct Biol*. 1996;3(5):410-413.

39. Nielsen EB, Schellman JA. The absorption spectra of simple amides and peptides. *J Phys Chem*. 1967;71(7):2297-2304.

40. Egholm M, Buchardt O, Christensen L, et al. PNA hybridizes to complementary oligonucleotides obeying the Watson-crick hydrogen-bonding rules. *Nature*. 1993;365(6446):566-568.

41. Paul A, Watson RM, Lund P, et al. Charge transfer through single-stranded peptide nucleic acid composed of thymine nucleotides. *J Phys Chem C*. 2008;112(18):7233-7240.

42. Mateo-Martí E, Briones C, Román E, Briand E, Pradier CM, Martín-Gago JA. Self-assembled monolayers of peptide nucleic acids on gold surfaces: a spectroscopic study. *Langmuir*. 2005; 21(21):9510-9517.

43. Wolak MA, Balaeff A, Gutmann S, et al. Electronic structure of self-assembled peptide nucleic acid thin films. *J Phys Chem C*. 2011;115(34):17123-17135.

44. Wöhlecke M, Borstel G. On the role of spin-orbit coupling and crystal symmetry on the spin-polarization of photoelectrons in nonmagnetic crystals. *Phys Scr*. 1983;T4:162-164.

45. Gersten J, Kaasbjerg K, Nitzan A. Induced spin filtering in electron transmission through chiral molecular layers adsorbed on metals with strong spin-orbit coupling. *J Chem Phys*. 2013; 139(11):114111.

46. Beall E, Ulku S, Liu C, et al. Effects of the backbone and chemical linker on the molecular conductance of nucleic acid duplexes. *J Am Chem Soc*. 2017;139(19):6726-6735.

47. Markus TZ, de Leon AR, Reid D, Achim C, Naaman R. The capture of low-energy electrons by PNA versus DNA. *J Phys Chem Lett*. 2013;4(19):3298-3302.

48. Parschau M, Ellerbeck U, Ernst KH. Chirality transfer by epitaxial mismatch in multi-layered homochiral molecular films. *Colloids and Surfaces A: Physicochem Eng Aspects*. 2010; 354(1-3):240-245.

49. Mishra S, Mondal AK, Pal S, et al. Length-dependent electron spin polarization in oligopeptides and DNA. *J Phys Chem C*. 2020;124(19):10776-10782.

50. Michaeli K, Naaman R. Origin of spin-dependent tunneling through chiral molecules. *J Phys Chem C*. 2019;123(27): 17043-17048.

51. Ghazaryan A, Paltiel Y, Lemeshko M. Analytic model of chiral-induced spin selectivity, J. Phys. *Chem C*. 2020;124(21): 11716-11721.

## SUPPORTING INFORMATION

Additional supporting information may be found online in the Supporting Information section at the end of this article.